Clays and Clay Minerals, Vol. 59, No. 1, 21–33, 2011.

THE FORMATION OF ILLITE FROM NONTRONITE BY MESOPHILIC AND THERMOPHILIC BACTERIAL REACTION

DEB P. JAISI[1,2], DENNIS D. EBERL[3], HAILIANG DONG[1], AND JINWOOK KIM[4,*]

[1] Department of Geology, Miami University, Oxford, OH 45056, USA
[2] Department of Plant and Soil Sciences, University of Delaware, Newark, DE 19716, USA
[3] US Geological Survey, Boulder, CO 80303, USA
[4] Department of Earth System Sciences, Yonsei University, Seoul, Korea

Abstract—The formation of illite through the smectite-to-illite (S-I) reaction is considered to be one of the most important mineral reactions occurring during diagenesis. In biologically catalyzed systems, however, this transformation has been suggested to be rapid and to bypass the high temperature and long time requirements. To understand the factors that promote the S-I reaction, the present study focused on the effects of pH, temperature, solution chemistry, and aging on the S-I reaction in microbially mediated systems. Fe(III)-reduction experiments were performed in both growth and non-growth media with two types of bacteria: mesophilic (*Shewanella putrefaciens* CN32) and thermophilic (*Thermus scotoductus* SA-01). Reductive dissolution of NAu-2 was observed and the formation of illite in treatment with thermophilic SA-01 was indicated by X-ray diffraction (XRD) and high-resolution transmission electron microscopy (HRTEM). A basic pH (8.4) and high temperature (65ºC) were the most favorable conditions for the formation of illite. A long incubation time was also found to enhance the formation of illite. K-nontronite (non-permanent fixation of K) was also detected and differentiated from the discrete illite in the XRD profiles. These results collectively suggested that the formation of illite associated with the biologically catalyzed smectite-to-illite reaction pathway may bypass the prolonged time and high temperature required for the S-I reaction in the absence of microbial activity.

Key Words—Illite-smectite Reaction, Microbial Fe(III) Reduction, NAu-2, *Shewanella putrefaciens* CN32, *Thermus scotoductus* SA-01.

INTRODUCTION

The formation of illite through the smectite-to-illite (S-I) reaction is considered to be one of the most important mineral reactions which occurs during the diagenesis of shale and mudstone (Peacor, 1992; Dong, 2005). Illite and smectite are often used as geothermometers (Weaver and Beck, 1971; Bethke *et al.*, 1988; Glasmann *et al.*, 1989) and geochemical indicators (Freed and Peacor, 1989; Lahann, 1980; Wintsch and Kvale, 1994) because the increase in the illite component of the I-S mixed layers is related to temperature (Hower *et al.*, 1976), time (Pytte and Reynolds, 1989), K concentration (Huang *et al.*, 1993), and water/rock ratio (Whitney, 1990). The extent of the S-I reaction, referred to as 'illitization', is linked to hydrocarbon maturation/migration (Burst, 1969; Peaver, 1999; Weaver, 1960), development of growth fault (Bruce, 1984), pore-water chemistry (Brown *et al.*, 2001), and changes in petrophysical properties such as rock cementation and porosity reduction (Bjørkum and Nadeau, 1998; Boles and Franks, 1979). For example, a reduction of 13% in the porosity and a 99% decrease in the permeability were reported when 80% of smectite was transformed to illite. As a result of the reaction, the typical random distribution of pores in smectite changed to a sub-parallel distribution with increasing illitization of smectite (Kim *et al.*, 1999). The extent of the S-I reaction is also used frequently as an independent geothermometer (Pollastro, 1993) to suggest the thermal history of sedimentary basins; this is useful in the exploration for methane hydrates associated with hydrocarbon seeps. Furthermore, the total clay layer charge increases from 0.25−0.60 to 0.6−0.9 per formula unit as smectite is reacted to illite. Layer charge is one of the important factors which controls the flocculation properties of clay suspensions (Kim *et al.*, 2005), which in turn affect the dynamic properties of sediments and, thus, influence mine burial as well as water-column optics.

The S-I reaction can occur either in solid-state (layer-by-layer replacement) or in solution (dissolution-precipitation). The layer-by-layer reaction mechanism is in the solid state, which implies a continuous increase in illite layers through a sequence of mixed-layer I-S phases, including smectite-rich R0, R1, R2, R3 I-S, and illite-rich I-S (Hower *et al.*, 1976). Several sets of transmission electron microscopy (TEM) results have demonstrated that smectite, R1 I-S (50% of illite layers in the mixed layers), and illite are dominant phases in the smectite−illite sequence (Ahn and Peacor, 1989; Veblen *et al.*, 1990; Kim *et al.*, 1995; Dong *et al.*, 1997).

* E-mail address of corresponding author:
Jinwook@yonsei.ac.kr
DOI: 10.1346/CCMN.2011.0590105

A lattice-energy calculation by Stixrude and Peacor (2002) confirmed these TEM observations and implied a reaction mechanism that involves dissolution of reactant smectite and precipitation of illite as a product. The variable geologic conditions in fluid composition, redox state, and the presence or absence of organic matter (Dong, 2005; Dong *et al.*, 2009) may lead to the different smectite-to-illite reaction mechanisms, though few studies until recently have taken into account the role of bacterial activity (Kim *et al.*, 2004; Zhang *et al.*, 2007a, 2007b; Dong *et al.*, 2009).

Recent studies have shown that bacteria are capable of reducing the structural Fe(III) in smectite under anaerobic conditions for respiration and growth (Gates *et al.*, 1993, 1998; Kim *et al.*, 2003; Kostka *et al.*, 1996, 1999a, 1999b; Stucki and Kostka, 2006; Seabaugh *et al.*, 2006; Jaisi *et al.*, 2005, 2007a, 2007b; Dong *et al.*, 2009). The features typical of dissolution/secondary phase precipitation associated with microbial reduction of structural Fe(III) in smectites were observed using TEM (Dong *et al.*, 2003). The biogenic smectite-to-illite reaction through microbial Fe(III) reduction at room temperature within 14 days (Kim *et al.*, 2004) indicated that (1) the microbial process may catalyze the S-I reaction and (2) a prolonged geologic time and elevated temperature, as required in the absence of microbial activity, may not be necessary. Zhang *et al.* (2007a, 2007b, 2009) and Vorhies and Gaines (2009) further tested this hypothesis under various conditions typical of those found in natural environments, *e.g.* by modifying the acidity of fluid, the amount of Al and K, the presence or absence of organic matter, and Fe contents in smectite clay minerals. However, the factors controlling the S-I reaction in biologically mediated redox condition are still not well known (Dong *et al.*, 2009). The objective of this study was, therefore, to test the microbially catalyzed S-I reaction, specifically under various conditions of temperature, solution chemistry, and aging of the redox reaction.

MATERIALS AND METHODS

The experimental design for microbial Fe(III) reduction in nontronite (NAu-2) by *Shewanella putrefaciens* CN32 and *Thermus scotoductus* SA-01 at various pH values and with or without supplemental Al content is summarized in Table 1.

Mineral, media, and reagent preparation

Clay-mineral preparation. The bulk sample of nontronite (NAu-2, $X_{0.72}(Si_{7.55}Al_{0.45})(Fe_{3.83}Mg_{0.05})O_{20}(OH)_4$, where X is Ca, Na, or K (Keeling *et al.*, 2000)) was purchased from the Source Clays Repository of The Clay Minerals Society. The <0.5 μm size fraction of NAu-2 was very pure (see below); the total structural Fe content was 23.4%, of which 99.8% was Fe(III). Details of the mineralogical and reactivity characterization of NAu-2 were discussed by Keeling *et al.* (2000) and Jaisi *et al.* (2005, 2007a, 2007b, 2008). First, the bulk sample was sonicated in an ultrasonic water bath to disperse loosely aggregated particles and then centrifuged to obtain the 0.02−0.5 μm size fraction in two steps: the ⩾0.5 μm particles were removed, and then the supernatant containing finer particles was centrifuged again to obtain particles in the 0.5−0.02 μm size range (using Stokes' settling law). The NAu-2 in this study was assumed to be free of Fe oxides, based on previous observations − the sample was devoid of any sextet in Mössbauer spectra at 12 K (Jaisi *et al.*, 2005). All the known Fe oxides (goethite, hematite, lepidocrocite, magnetite, ferrihydrite, *etc.*) display sextets at 12 K, irrespective of whether they are pure (Murad and

Table 1. Experimental set up for Fe(III) reduction, microscopy, and XRD analysis.

Bacteria type	pH	Culture	External Al source (5 mM)	Microscopy sample: TEM Resin	Microscopy sample: SEM Air-dried	— Sample treatment for XRD — Air-dried	Glycolated	Li-saturated	Li-sat glycolated
Shewanella CN32	6.2 (±0.15)	Growth	N			X	X		
	7.1 (±0.25)	Growth	N			X	X		
	8.4 (±0.2)	Growth	N			X	X		
	6.2 (±0.15)	Growth	Y			X	X		
	7.1 (±0.25)	Growth	Y	X	X	X	X	X	X
	8.4 (±0.2)	Growth	Y			X	X	X	X
Thermus SA-01	6.4 (±0.2)	Non-growth	N			X	X		
	8.1 (±0.1)	Non-growth	N			X	X		
	6.4 (±0.2)	Non-growth	Y			X	X		
	8.1 (±0.1)	Non-growth	Y			X	X		
	6.4 (±0.2)	Growth	N			X	X		
	8.1 (±0.1)	Growth	N			X	X		
	6.4 (±0.2)	Growth	Y	X	X	X	X	X	X
	8.1 (±0.1)	Growth	Y	X	X	X	X	X	X

https://doi.org/10.1346/CCMN.2011.0590105 Published online by Cambridge University Press

Cashion, 2004), nanosized (*e.g.* goethites; Larese-Casanova *et al.*, 2010), substituted with any diamagnetic cations (*e.g.* Fe for Al) (Fysh and Clarke, 1982), or coated with diamagnetic cations (*e.g.* Si; Zhao *et al.*, 1996). Jaisi *et al.* (2005) published a ±4 mm/s Mössbauer spectrum of the original NAu-2 at 12 K which showed no characteristics of Fe oxides (Jaisi *et al.*, 2005). The substitution of cations or coatings would affect the magnetic ordering but all displayed a sextet at 12 K (unpublished data).

Bacterial strain and media preparation. *Shewanella putrefaciens* CN32, a gram-negative facultative bacterium, is commonly present in groundwater and has been found capable of reducing Fe(III) in various environments (Fredrickson *et al.*, 1998; Lovley *et al.*, 2004). *S. putrefaciens* CN32 was grown aerobically in tryptic soy broth (TSB) (30 g/L) until the mid- to late-log phase and was washed three times in bicarbonate buffer (2 g/L of reagent-grade $KHCO_3$ and 0.1 g/L KCl) at room temperature. The washed cells were re-suspended in the M1 medium (see below) and the initial cell density was determined by both optical-density measurement and viable-cell count. All chemicals containing Na in the growth media were replaced with K equivalents in order to promote the smectite-to-illite reaction. The composition of the M1 medium for CN32 cells (Fredrickson *et al.*, 1998) was as follows: 22 mM NH_4Cl, 12 mM KCl, 0.61 mM $CaCl_2$, 0.71 mM of nitrilotriacetic acid, 1.1 mM $MgSO_4.7H_2O$, 1.5 mM NaCl, 0.27 mM $MnSO_4.H_2O$, 86 μM $ZnCl_2$, 32 μM $FeSO_4.7H_2O$, 61 μM $CaCl_2.2H_2O$, 38 μM $CoCl_2.6H_2O$, 9.3 μM $Na_2MoO_4.2H_2O$, 6.8 μM $Na_2WO_4.2H_2O$, 9.1 μM $NiCl_2.6H_2O$, 3.6 μM $CuSO_4.5H_2O$, 1.9 μM $AlK(SO_4)_2.12H_2O$, and 15 μM H_3BO_3 with treatment-specific components 27 mM $KHCO_3$, 4.5 mM of 1,4-piperazinediethanesulfonic acid, and 3.9 mM KH_2PO_4.

Thermus scotoductus SA-01, a thermophilic bacterium (Kieft *et al.*, 1999; Balkwill *et al.*, 2004; Moller and van Heerden, 2006), was provided by Dr. Tom Kieft (New Mexico Institute of Mining and Technology, USA). SA-01 was grown aerobically at 65ºC in the TYG medium consisting of 5.0 g of tryptone, 3.0 g of yeast extract, and 1.0 g of glucose per liter of H_2O. The complex growth medium for SA-01 was prepared by mixing 10 mL of 10× Wolfe's trace element solution and 15 mL of 10× Wolfe's vitamins per liter of basal medium (Kieft *et al.*, 1999). The composition of the basal medium was (per liter of deionized water) 0.42 g KH_2PO_4, 0.22 g K_2HPO_4, 0.2 g NH_4Cl, 0.38 g KCl, 0.36 g KCl, 0.04 g $CaCl_2{\cdot}H_2O$, 0.1 g $MgSO_4{\cdot}7H_2O$, 1.8 g $KHCO_3$, 0.5 g K_2CO_3, and 0.19 mg Na_2SeO_4. The 10× Wolfe's vitamin solution contained (per liter of deionized water) 2.0 mg biotin, 2.0 mg folic acid, 10.0 mg pyridoxine HCl, 5.0 mg riboflavin, 5.0 mg thiamine, 5.0 mg nicotinic acid, 5.0 mg pantothenic acid, 0.1 mg cyanocobalamin, 5.0 mg p-aminobenzoic acid, and 5.0 mg thioctic acid. The 10× Wolfe's mineral solution contained (per liter of deionized water) 2.14 g nitrilotriacetic acid (NTA), 0.1 g $MnCl_2{\cdot}4H_2O$, 0.3 g $FeSO_4{\cdot}7H_2O$, 0.17 g $CoCl_2{\cdot}H_2O$, 0.2 g $ZnSO_4{\cdot}7H_2O$, 0.03 g $CuCl_2{\cdot}2H_2O$, 5 mg $KAl(SO_4)_2{\cdot}12H_2O$, 5 mg H_3BO_4, 0.09 g Na_2MoO_4, 0.11 g $NiSO_4{\cdot}6H_2O$, and 0.02 g $Na_2WO_4{\cdot}2H_2O$. In this experiment, the possibility of clay dissolution (Kostka *et al.*, 1999) was not considered. Serial dilution and growth of SA-01 cells from its original stock solution were performed to accommodate its metabolism with a solid-state electron acceptor (*i.e.* Fe(III) in NAu-2). For each successive dilution step, SA-01 cells from an old culture were transferred to a fresh NAu-2 solution that had a greater concentration of NAu-2. Cell growth and adaptation at a particular NAu-2 concentration was continued for 7−10 days. The cells grown from the third generation were used in the experiment.

Bioreduction experiment

Bioreduction experiments were performed at various pH conditions ranging from 6.2 to 8.4. Nontronite (NAu-2) stock suspension was prepared in the respective buffers/media at a concentration of 50 mg/mL and sterilized by autoclaving. Filter-sterilized vitamins and temperature-sensitive mineral supplements were added after autoclaving of the other components of the media. The Fe(III) reduction experiments were performed with Fe(III) in NAu-2 as the sole electron acceptor (~21 mmol/L) and lactate as the electron donor (20 mM) in the presence of an electron shuttling compound anthraquinone-2, 6-disulfonate (AQDS) (0.1 mM). Each experimental tube received ~2×10^8 cells/mL (final concentration) and media/buffer amendments (as above) and was sealed with a thick butyl rubber stopper after purging with N_2/CO_2 gas mix (80:20). The final experimental pH was adjusted using 0.5 N HCl and NaOH during purging. Supplemental Al (5 mM, as $Al_2(SO_4)_3$) was added to selected experiments to understand the role and requirement of Al for the formation of illite. For CN32, a bioreduction experiment in a growth medium (M1) was conducted. For SA-01, both non-growth (bicarbonate buffer) and growth (the above complex medium) experiments were conducted. All experiments were performed in duplicate in 20 mL final volume. Control experiments were identical to the other experiments but used an equivalent volume of buffer/medium instead of cells. Experiments with CN32 cells were incubated at 30ºC with shaking at 60 rpm and those of SA-01 cells were incubated at 65ºC with manual shaking once a day.

Extent of Fe(III) reduction

The extent of microbial reduction of Fe(III) in nontronite was monitored by measuring the HCl-extractable Fe(II). At select time points, 0.5 mL of

https://doi.org/10.1346/CCMN.2011.0590105 Published online by Cambridge University Press

mineral suspension was treated with 0.5 N HCl for 24 h and the extracted Fe^{2+} was measured by the Ferrozine method (Stookey, 1970). The 0.5 N HCl extraction method has been shown to extract some, but not all, of the microbially produced Fe(II) in phyllosilicates (Jaisi *et al.*, 2007a, 2007b; Anastacio *et al.*, 2008). As a result, the extent of Fe(III) reduction calculated is underestimated by an unknown amount.

X-ray diffraction (XRD)

Residual nontronite in both the control and bioreduction experiments was characterized by XRD to identify mineralogical changes as a result of bioreduction. The ethylene glycolation technique (Moore and Reynolds, 1997) was applied to identify illite. The 80–100 mg clay samples were dispersed in 1 mL of distilled water using an ultrasonic water bath and then Li-saturated. An oriented nontronite thin film was then prepared by repeated pipetting of the clay suspension onto a glass slide and then air-dried. Samples were scanned with a Siemens D500 X-ray diffractometer with CuKα radiation in 0.02 or 0.05º2θ steps from 2 to 35º2θ, with a count time of 2 s per step.

Measurement of illite particle thickness

Samples showing the presence of mixed-layer illite-smectite (from XRD results) were tested again after saturating twice with 1 mol/L LiCl to understand if the mixed stratifications were permanent. Those samples having permanent K-fixation were further analyzed to determine the thickness distribution of illite particles as a function of solution chemistry using the method described in Eberl *et al.* (1998). In brief, a dilute suspension of reduced NAu-2 was saturated with PVP (polyvinyl pyrrolidone, molecular weight 10,000). The sample was sonicated for maximum preferred orientation and then hardened in Si-metal wafers that were cut perpendicular to (100) to reduce the background XRD intensity (Eberl *et al.*, 1998). This method eliminates inter-particle diffraction and therefore allows quantification of illite particle thickness from the broadening of the 001 peaks (Blum and Eberl, 2004). The 00*l* peaks were then used for measurement of mean particle thickness and thickness distribution (Drits *et al.*, 1997, 1998) using the *MudMaster* program (Eberl *et al.*, 1996). This procedure has been demonstrated by Kim *et al.* (2004) to identify the illite and its crystal-size distribution.

Scanning and high-resolution transmission electron microscopy (SEM and HRTEM)

Mineralogical changes were further studied using SEM and HRTEM. The SEM samples were prepared following a previously published procedure (Dong *et al.*, 2003). Briefly, cell-mineral suspensions were fixed in 2.5% glutaraldehyde in bicarbonate buffer and one droplet of fixed suspension was placed on the surface of a glass cover slip that had been cleaned with 1 mg/mL of poly-E-lysine solution prior to use. The nontronite particles were allowed to settle onto the cover slip for 15 min. The sample-coated cover slip was dehydrated sequentially using varying proportions of ethanol and distilled water followed by critical-point drying. The cover slip was mounted onto a SEM stub and coated with Au. The sample was then analyzed using a Zeiss Supra 35 FEG-VP SEM at an accelerating voltage of 10–15 kV at a working distance of 6–10 mm. However, the working distance and beam current were increased to 8 mm and 60–70 μA, respectively, for energy dispersive spectroscopy (EDS) analysis. The intensity of elemental peaks in the EDS patterns was analyzed qualitatively based on the atomic proportion of the elements in the mineral (smectite/illite) and their atomic weight.

For HRTEM analysis, both abiotic control and bioreduced solid samples were embedded in hydrophilic Nanoplast® resin using the method described by Kim *et al.* (2003, 2004). The method does not require solvent exchange (methanol/water exchange) and, therefore, minimizes any artifacts during sample preparation. A JEOL 3010 TEM operating at 300 keV with a LaB_6 filament was used for all of the HRTEM analyses. Imaging experiments were performed at high magnification (up to 400 k) to resolve fine lattice fringes associated with secondary mineral phases.

RESULTS

Microbial reduction of Fe(III) in nontronite

Shewanella putrefaciens CN32. The extent of bioreduction in bioreduced NAu-2, without addition of supplemental Al in the growth medium, reached up to 18% after 8 days and leveled off after reaching 22–35% in 13 days, depending on the pH (Figure 1a). The maximum extent of Fe(III) reduction occurred at pH 7.1. Similar degrees of Fe(III) reduction at various pH values were reached in the presence of supplemental Al (5 mM) but with slower rates (Figure 1b). No measurable Fe(III) reduction was detected in control experiments.

Thermus scotoductus SA-01. Although several transfers of the original SA-01 culture were performed to enable its adaptation to the solid-state electron acceptor in NAu-2, a significant lag phase was still observed in Fe(III) reduction experiments. The lag time varied from 9 to 23 days in the non-growth medium (Figure 1c) and from 6 to 8 days in the growth medium (Figure 1d). The extent of Fe(III) reduction at pH 8.1 and 6.4 after 123 days of incubation was 9.0 and 21.5%, respectively, though the addition of supplemental Al at each pH value decreased the extent of Fe(III) reduction slightly (2–4 %) in both growth and non-growth experiments. A significant, pH-dependent decrease in the extent of

https://doi.org/10.1346/CCMN.2011.0590105 Published online by Cambridge University Press

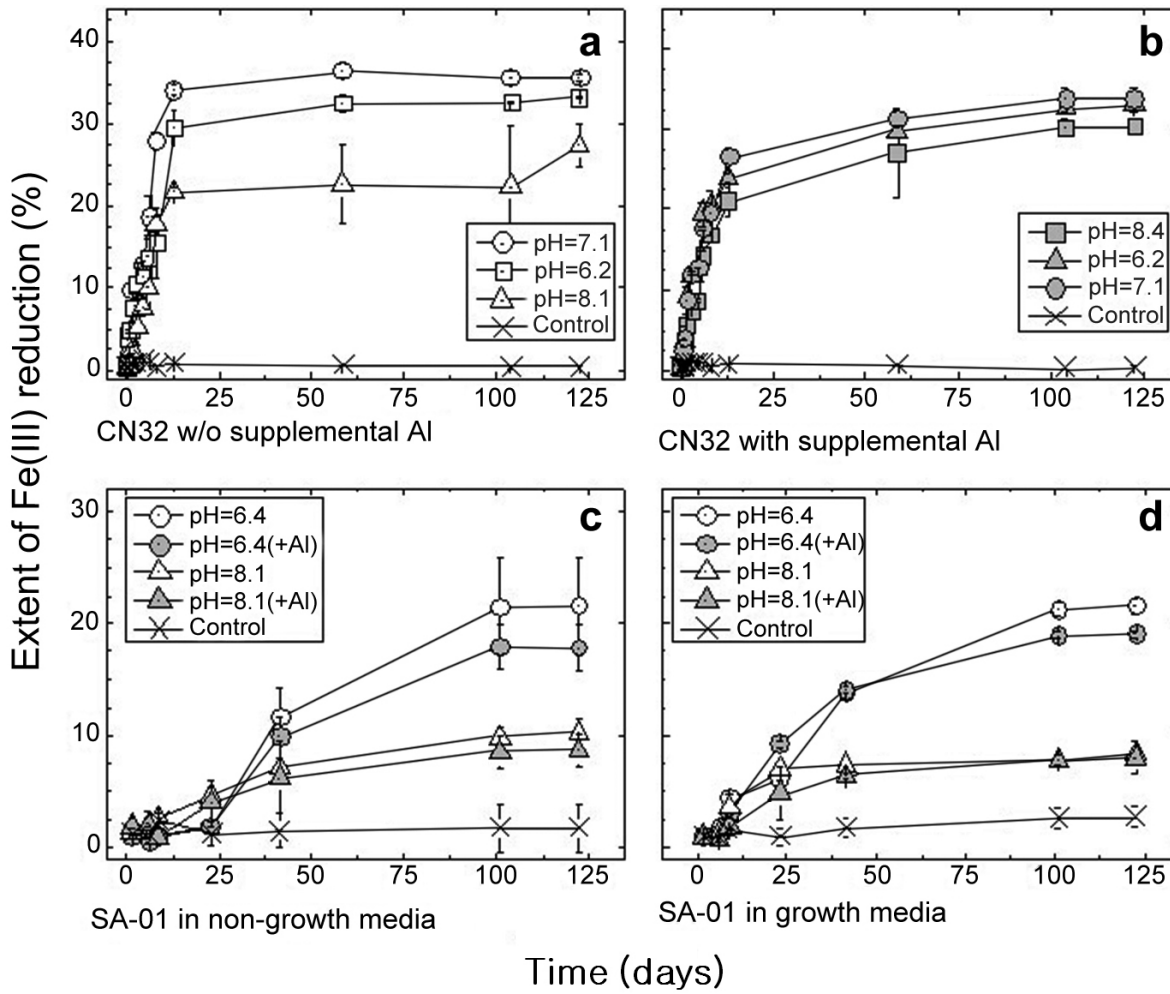

Figure 1. Extent of Fe(III) reduction in NAu-2 as a function of time in the presence of CN32 and SA-01: CN32 cells incubated in the M1 growth medium without external Al source (a) and with supplemental 5 mM external Al (b). SA-01 cells were grown in non-growth (c) and growth (d) media with and without supplemental Al, as indicated. All experiments were performed at pH 6.2, 7.1, or 8.5 and in duplicate.

Fe(III) reduction was observed (9% at pH 8.1 compared to 17.5–21.5% at pH 6.4 regardless of supplemental Al content). No appreciable Fe(III) reduction was measured in the control experiments.

X-ray diffraction

S. putrefaciens CN32. The XRD profiles (Figure 2) for the microbially Fe(III)-reduced nontronite samples at pH 7.1 for the 13-day incubation period at room temperature (samples with supplemental Al (+Al), Li-saturation (Li), and ethylene-glycolation (Gly)) were examined for any signs of illite formation associated with microbial Fe(III) reduction. The abiotic control sample (Control) displayed a 9.8 Å peak that was shifted to a broad peak of 14.5 Å upon glycolation (Gly-control). The air-dried/bioreduced samples (Bioreduced, Bioreduced (+Al), Li-bioreduced, and Li-bioreduced (+Al)), regardless of supplemental Al content or Li-saturation, showed peaks only at ~10 Å. Upon glycolation, the 10 Å peak was split into 15.8 and 9.7 Å peaks for the bioreduced sample regardless of the presence or absence of supplemental Al (Gly-bio-reduced, Gly-bioreduced (+Al)), and into 16.6 and 8.6 Å peaks for the Li-saturated, bioreduced samples (Gly-Li-bioreduced, Gly-Li-bioreduced (+Al)).

The XRD profiles (Figure 3) for the microbially Fe(III)-reduced nontronite samples at pH 8.2 for the 6-month incubation period (the air-dried Control and Control (+Al) samples, as well as the Bioreduced and Bioreduced (+Al) samples) all showed a 10 Å peak. Upon glycolation treatment, broad peaks at 12.6–12.8 Å and 10.1 Å were observed for the control samples. Peaks at 10 Å and 15.3 Å were clearly observed in the Bioreduced (+Al) samples and peaks at 10 Å and 12.7 Å in the Bioreduced samples.

https://doi.org/10.1346/CCMN.2011.0590105 Published online by Cambridge University Press

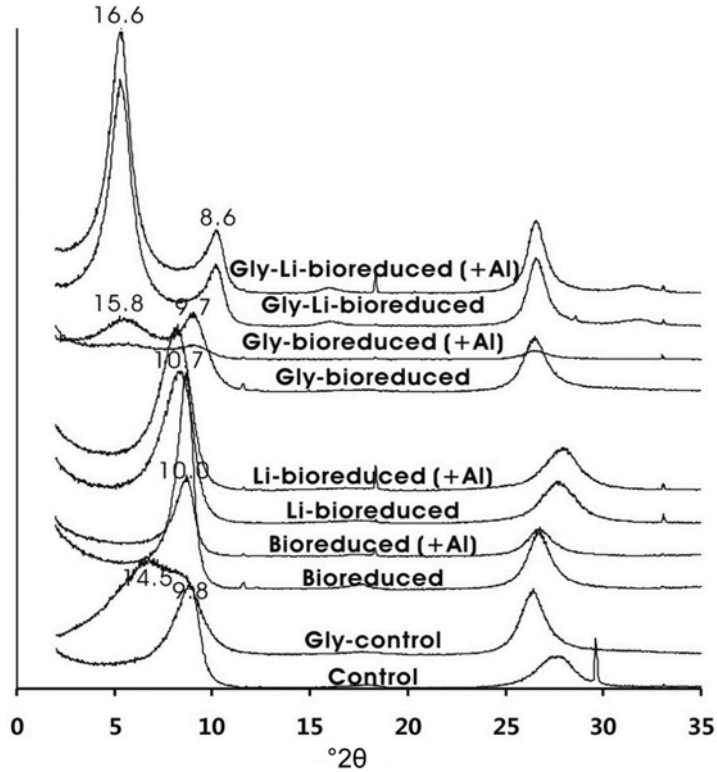

Figure 2. XRD patterns of bioreduced NAu-2 incubated for 13 days with CN32 cells at 30ºC. The experiments were performed at pH 7.1 with (5 mM) and without supplemental Al. The XRD patterns include air-dried, glycolated (Gly), or Li-saturated bioreduced samples with additional supplemental Al (+Al) and control sample. The XRD profiles for the abiotic control sample (Control) displayed a 9.8 Å peak that was shifted to 14.5 Å upon glycolation (Gly-control). The air-dried/bioreduced samples (Bioreduced, Bioreduced (+Al), Li-bioreduced, and Li-bioreduced (+Al)) showed a peak at ~10 Å. Upon glycolation, the 10 Å peak was split into 15.8 and 9.7 Å peaks for the bioreduced sample, and into 16.6 and 8.6 Å for the Li-saturated, bioreduced samples (Gly-Li-bioreduced, Gly-Li-bioreduced (+Al)).

Thermus scotoductus (SA-01). The XRD profiles (Figure 4) for the microbially Fe(III)-reduced nontronite samples at pH 8.1 for the 6-month incubation period at 65ºC revealed that a peak is present at ~10 Å in the Bioreduced and Bioreduced (+Al) samples, similar to that for the Control sample. Upon glycolation, the 10 Å peak shifted to 12.7 Å for the Control, while it was split into 13.5 Å and 10 Å for the Bioreduced sample. In the Gly-bioreduced (+Al) sample the 10 Å separated into a 14.3 Å and a 10 Å peak. Upon glycolation of the bioreduced samples, followed by Li saturation, both 11.3 Å (+Al) and 10.8 Å (−Al) peaks were split into 17.1 Å and 8.7 Å (Figure 5). Furthermore, a low-intensity peak was detected at ~10 Å in both profiles for bioreduced samples only. After the PVP treatment of the same samples, the 10 Å peak intensified (inset in Figure 5). These X-ray profiles (gycolated and Li-saturated samples of bioreduced NAu-2 by SA-01 for 6 months) were further characterized using the *Mudmaster* program. The individual crystallites (corresponding to the intensified 10 Å peak after the PVP treatment) clearly revealed mean thickness and thickness distributions that varied from 1 to 10 nm (Figure 6).

Transmission/scanning electron microscopy

The TEM images of the control and bioreduced nontronites by SA-01 for 6 months (Figure 7) indicated that, for the control samples, nontronite particles were aggregated with 1.2 nm d_{001} lattice fringes, which were consistent with the selected area electron diffraction (SAED) pattern (Figure 7a, inset) of the outlined area (Figure 7a). The diffuse-ring nature of the SAED patterns reflected a disoriented, aggregated arrangement of nontronite particles. The TEM image of the bioreduced samples displayed a discrete illite-like packet with 1.0 nm spacing corresponding to the accompanying SAED patterns (Figure 7b,c and insets). A packet of 12 layers 1.0 nm thick was measured (Figure 7c). Observation of mineral grains in the bioreduced nontronite sample by SEM-EDS suggested the presence of both primary and secondary minerals (Figure 8). For example, elemental compositions of morphologically distinct parts of an aggregate measured by EDS showed the presence of Al, Si, K, and Ca from grain A/B, Si and Ca from grain C, and only Si contents from grain D/E. Although the EDS results were qualitative, a preliminary

https://doi.org/10.1346/CCMN.2011.0590105 Published online by Cambridge University Press

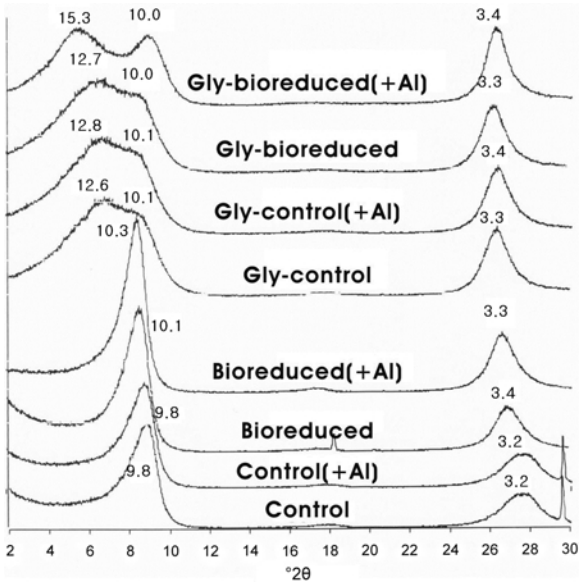

Figure 3. XRD patterns of bioreduced NAu-2 after 6 months of incubation with CN32 cells at 30ºC. The experiments were performed at pH 8.2 with (5 mM) and without supplemental Al. The XRD patterns include air-dried and glycolated (Gly) bioreduced samples with additional supplemental Al (+Al) and control sample. The air-dried control samples (Control and Control (+Al)) and bioreduced samples (Bioreduced and Bioreduced (+Al)) showed a 10 Å peak. Upon glycolation treatment, peaks at 12.6–12.8 Å and 10.1 Å appeared for the control samples. The peaks at 10 Å and 15.3 Å were observed for the bioreduced sample with supplemental Al.

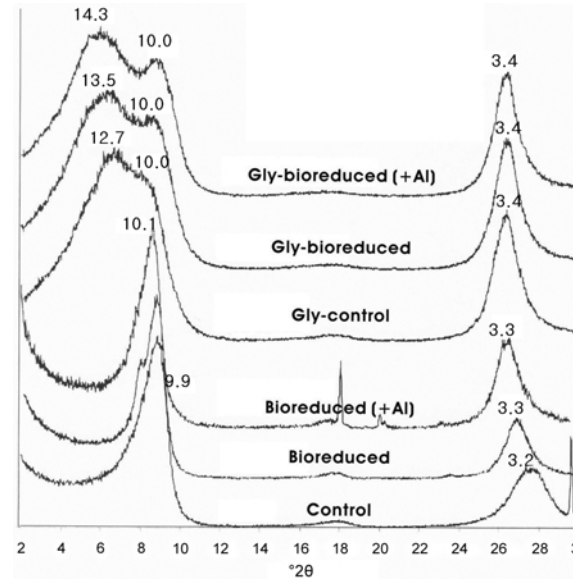

Figure 4. XRD patterns of bioreduced NAu-2 after 6 months of incubation with SA-01 cells at 65ºC. The experiments were performed at pH 8.1 with (5 mM) and without supplemental Al. The XRD patterns include air-dried and glycolated bioreduced samples with (5 mM) and without supplemental Al and control sample. A peak at ~10 Å was observed in both the bioreduced samples (Bioreduced (+Al), Bioreduced) and the control sample (Control). Upon glycolation, the 10 Å peak was shifted to 12.7 Å for the control sample, while it was split into 13.5 Å and 10 Å for the bioreduced sample (Bioreduced). In the bioreduced samples with a supplemental Al content (Gly-bioreduced (+Al)), the peak was split into 14.3 Å and 10 Å peaks.

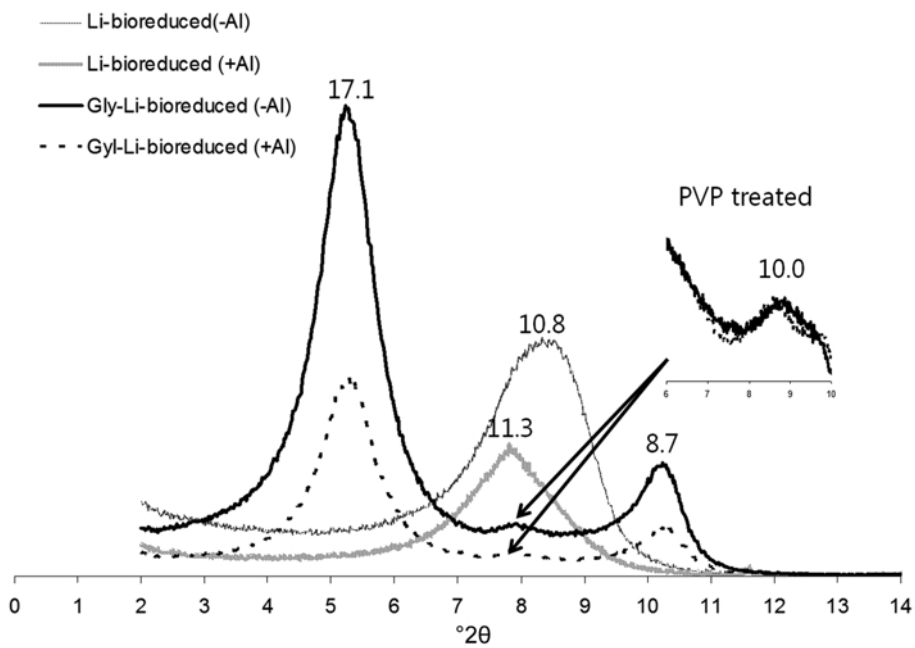

Figure 5. XRD patterns of bioreduced NAu-2 after 6 months of incubation with SA-01 cells at 65ºC. The experiments were performed at pH 8.1 with (5 mM) and without supplemental Al. The XRD patterns include air-dried and glycolated bioreduced samples followed by Li saturation displaying peaks at 11.3 Å (+Al) and 10.8 Å (−Al) separated to 17.1 Å and 8.7 Å. The sample was then treated with polyvinyl pyrrolidone (PVP) resulting in the appearance of the intensified 10 Å peak (inset) suggesting discrete illite.

https://doi.org/10.1346/CCMN.2011.0590105 Published online by Cambridge University Press

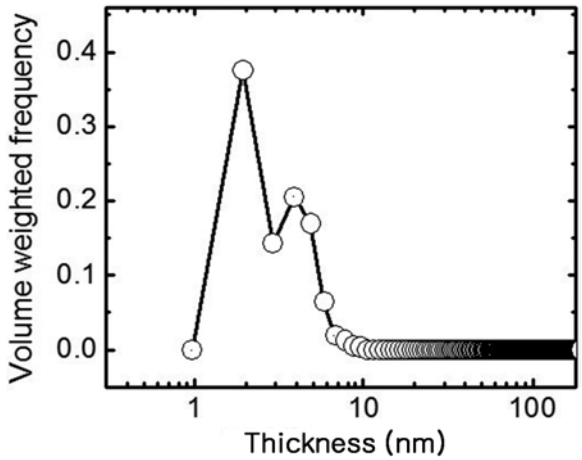

Figure 6. Thickness of an illite crystallite formed in a sample incubated with SA-01 for 6 months. The thickness distribution was calculated using the *MudMaster* model.

estimate, based on the Al/Si ratio and K content, suggests that the mineral in spot A was probably illite with Ca possibly a residual ion from the SA-01 growth media. Grain C was identified as calcite, and D and E were silica precipitates. Whether the Na detected on spot A was from the residual media or was present from original NAu-2 is unclear. Some layers with Na may still be present even if all nontronite was assumed to be K-homoionic.

DISCUSSION

Characteristics of microbially Fe(III)-reduced nontronite by XRD

Observed shifts in the XRD peak in both the control samples and in samples bioreduced by CN32 cells (Figures 2, 3) were probably caused by non-permanent K-fixation in bioreduced nontronite layers. The layers (~10 Å) of the bioreduced nontronite samples (Figures 2,

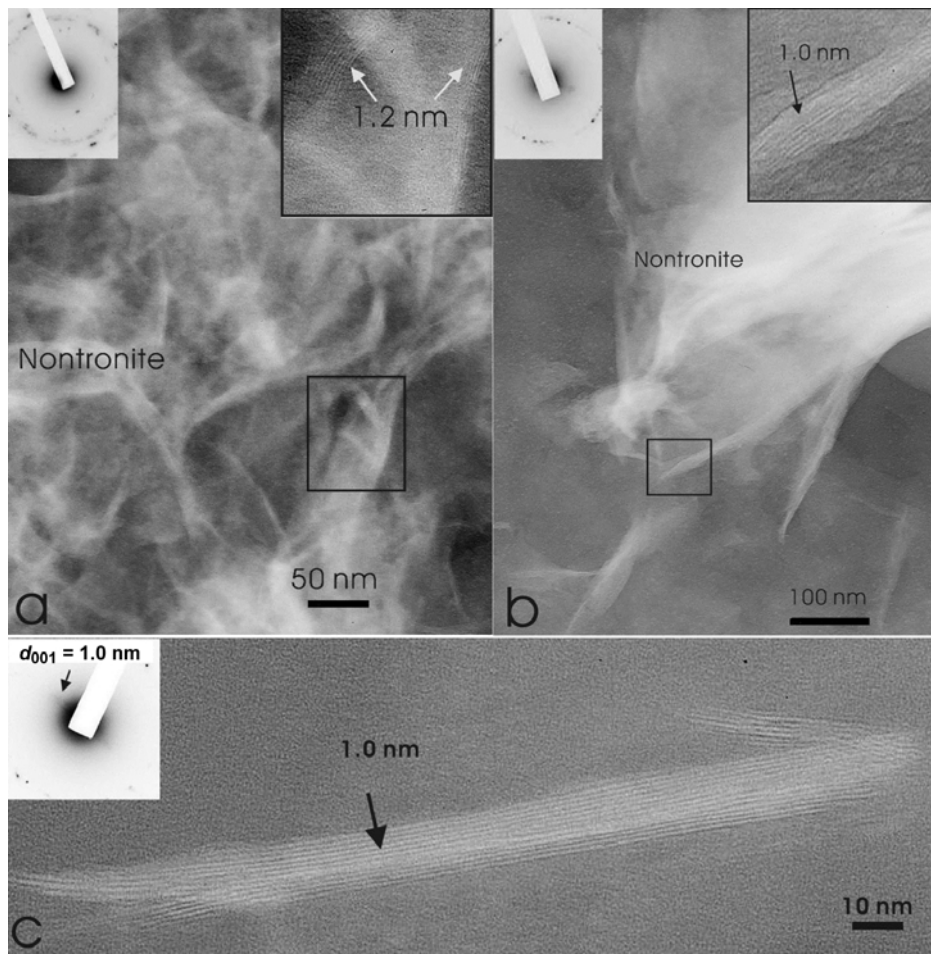

Figure 7. TEM images of control sample (a) and bioreduced samples (b,c) incubated for 6 months with SA-01 at pH 8.1 showing 1.2 nm d_{001} lattice fringes corresponding to the inset selected area electron diffraction (SAED) pattern of the outlined area in part a and a discrete illite-like packet with 1.0 nm spacing corresponding to the inset SAED patterns in parts b and c.

https://doi.org/10.1346/CCMN.2011.0590105 Published online by Cambridge University Press

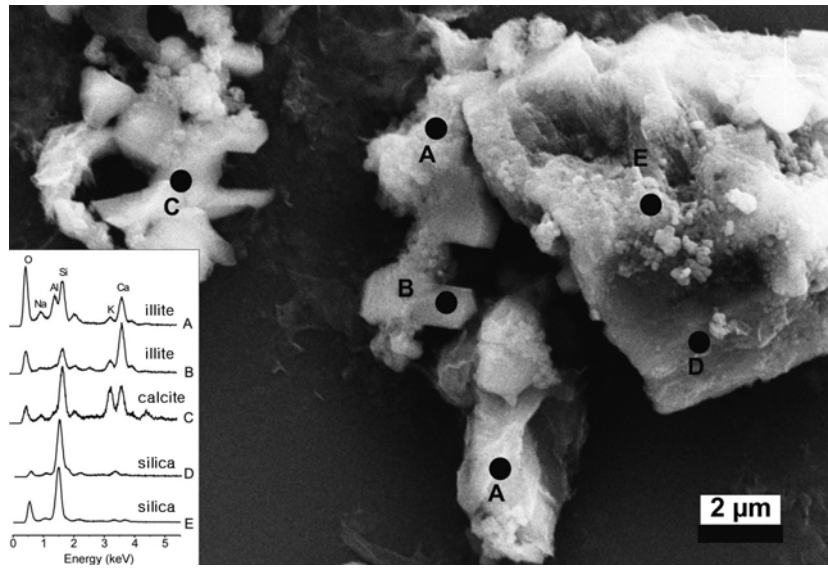

Figure 8. SEM image of bioreduced NAu-2 incubated for 6 months with SA-01 at pH 8.1. Various mineral phases produced as a result of Fe(III) reduction are indicated in the EDX spectra.

3) may be due to layer collapse associated with K-fixation (K-homoionization) because the 10 Å layer was also observed in control samples. Furthermore, the 10 Å peak of Li-saturated bioreduced nontronite, upon glycolation, separated to 16.6 and 8.6 Å, indicating that the K was not permanently fixed in the interlayer as required for illite formation, and the two separated peaks at 16.6 and 8.6 Å may correspond to the d_{001} and d_{002} values, respectively. Upon glycolation, the 10 Å and 15.3 Å peaks (Figure 3) and 10 Å and 14.3 Å peaks (Figure 4) were clearly separated in the bioreduced samples with supplemental Al, suggesting that the presence of Al in bioreduced nontronite may form the Al-rich nontronite with a low layer-charge density but may result in greater interlayer expansion upon glycolation. Kaufhold and Dohrmann (2010) demonstrated that K-smectite (layer-collapsed smectite) can be formed depending on the layer-charge density, and the peak separation by the glycol-solvation technique may not be a sufficient indication of illite formation. Indeed, calculation of the Gly-Li-bioreduced X-ray profiles (Figure 2) by *NEWMOD*© (Reynolds, 1985) indicated that the pattern may have contained 10–15% of 10 Å layers in a mixed-layer illite-smectite with R0 ordering (not shown) and these layers may not be discrete illite. The occurrence of the 10 Å peak does not, therefore, necessarily mean that illite was formed (Kaufhold and Dohrmann, 2010). Other tests are needed to confirm its presence.

The XRD traces of the bioreduced sample (not Li-saturated) incubated for 6 months with SA-01 displayed a 10 Å peak separation upon glycolation. Upon Li saturation and glycolation, the same sample exhibited a 10 Å peak, characteristic of typical illite, which was confirmed by the PVP treatment (see the inset XRD profiles in Figure 5). Measurement of the illite:smectite ratio based on peak migration from 26º to 27º2θ (3.42 to 3.29 Å) and from 15.4º to 17.7º2θ (5.74 to 5.0 Å) (Method III, Środoń, 1980) upon ethylene glycol solvation plotted data outside of the published calibrated field (which limits only up to 60% smectite), suggesting that only a small fraction of NAu-2 was changed to illite.

The size distribution of the newly formed illite crystallites, as determined by XRD, was asymptotic in nature. The packet thickness distribution of illite (120 Å) measured from HRTEM, however, was different from that calculated from the *Mudmaster* program (95% for 20–50 Å layers and <5% for ~70–90 Å layers) (Figure 6). The discrepancy between XRD and TEM results may be due to the same problems that were addressed controversially in the explanation of the S-I reaction mechanism (Ahn and Peacor, 1989; Kim *et al.*, 1995; Dong *et al.*, 1997) and may be related to the different sensitivities of X-ray *vs.* electron beams to detect structural coherency. If two adjacent layers are rotated by <15º around *c**, the TEM may sense the interface as coherent, but XRD may detect it as incoherent. Because XRD has such a long wavelength, it is unable to detect specific interfaces, as TEM can. X-ray diffraction, therefore, senses the correct ratio of layers, but cannot identify specific sequences as well as the shorter-wavelength TEM can (Dong, 2005).

Secondary-phase mineral precipitation

The secondary-phase minerals such as silica (grain D) and calcite (grain C) detected by SEM-EDS may have resulted from dissolution of bioreduced nontronite associated with microbial Fe(III) reduction, consistent with previous results (Li, H., *et al.*, 2004, Zhang *et al.*,

https://doi.org/10.1346/CCMN.2011.0590105 Published online by Cambridge University Press

2007a, 2007b; Jaisi *et al.*, 2005, 2008; Furukawa *et al.*, 2007). Particles >2.0 μm are shown in Figure 8 but whether these are the result of newly precipitated minerals or aggregates of existing mineral grains is unclear. Calcite precipitation was observed in a previous study of microbial reduction of Fe(III) in nontronite by a sulfate-reducing bacterium (Li, Y.L., *et al.*, 2004), and has yet to be clearly explained. In the present study, calcite could have been produced by the media used in the bioreduction experiment. The release of silica has been suggested to be related to the S-I reaction in natural geochemical environments (Cuadros and Linares, 1998; Cuadros, 2006; Vorhies and Gaines, 2009). Amorphous Si precipitation in bacterial Fe(III) reduction in nontronite has been found to be extensive under some circumstances and may not necessarily be related to the formation of illite layers (Furukawa and O'Reilly, 2007).

Factors controlling the microbially mediated S-I reaction

The extensive number of experiments performed in this study lend themselves to a greater understanding of the major factors controlling the S-I reaction.

pH. As the type of bacteria chosen for the reduction experiments in this study were slightly acidophilic (SA-01) or neutrophilic (CN32), their ability to cause an Fe respiration process at higher pH values (~8.1−8.4) may have been compromised, resulting in a lesser extent of Fe(III) reduction compared with lower pH (~6.2−7.1) (Figures 1, 2). Illite layers were not formed when the extent of reduction was 21.5% at acidic pH (pH 6.4 after 6 months of incubation with SA-01). Illite formation was detected, however, in samples with only 8−10% of Fe(III) reduction at alkaline pH (pH 8.1 with SA-01 for 6 months of incubation). The results suggested that the formation of illite layers is favored by alkaline pH, as consistent with published results on the S-I reaction catalyzed by a thermophilic bacterium *Thermoanaerobacter ethanolicus* (Zhang *et al.*, 2007b). Indeed, previous research demonstrated that increasing the pH can enhance smectite dissolution (Bauer and Velde, 1999; Claret *et al.*, 2002) and illite formation (Eberl *et al.*, 1986, 1993; Drief *et al.*, 2002).

Al content. The source of Al for illitization may be derived from dissolution or 'cannibalism' of smectites rather than external sources such as dissolution of K-feldspar in natural geochemical environments (Boles and Frank, 1979; Pollastro, 1985). The stoichiometric calculation showed that the amount of additional Al required (other than that already present in NAu-2) to convert all smectite to illite is 0.113 g of Al/g of NAu-2 (*i.e.* 2.1 mM of Al for our experiments performed at 5 g/L NAu-2 concentration). The amount of Al added (5 mM) in the present experiments was, therefore, in excess, allowing for a 1:1 dissolution of NAu-2 and precipitation of illite. At high temperature (experiments with SA-01), illite layers were formed in the reduction experiments regardless of Al supplement (Figure 5), suggesting that the addition of Al might enhance the S-I reaction but may not be an essential condition. The results are consistent with previous results using the thermophilic bacterium *Thermoanaerobacter ethanolicus* (Zhang *et al.*, 2007b).

Temperature and time. The layers with ~10 Å spacing observed in the samples incubated with CN32 for 13 days at 30ºC may have resulted from the collapse due to K-saturation. This may also represent high-charged smectite due to microbial Fe(III) reduction (Gates *et al.*, 1998; Liu *et al.*, 2010) or K-smectite (Kaufhold and Dohrmann, 2010) rather than permanently fixed layers. The small increase in layer charge may not be sufficient to overcome the hydration energy of interlayer cations (Howard, 1981). The high-charge smectite layers were re-expanded upon glycolation (Figures 2, 3). The formation of permanent 10 Å layers for the longer incubation period (6 months) with SA-01 at 65ºC (Figure 5) suggests that the S-I reaction is favored either by a sufficiently long incubation period or by a high temperature of reaction.

CONCLUSION

The extent of microbial reduction of Fe(III) in pure nontronite differed greatly depending on the bacterium, temperature, pH, solution chemistry, and time. Because these bacteria were neutrophilic or slightly acidophilic and higher pH inhibited their metabolic activity, the extent of reduction was less at higher pH. The formation of illite layers that are distinct from K-nontronite was found to be independent of the extent of reduction and was favored at high pH and temperature. The reaction time was an important factor when temperature was low. The presence of additional Al may not be essential to enhance the S-I reaction.

ACKNOWLEDGMENTS

The present research was supported by the Basic Science Research Program through the National Research Foundation of Korea (NRF) funded by the Ministry of Education, Science and Technology (20090085989) to JWK, a grant from the National Science Foundation (EAR-0345307) to HD, and by student grants from The Clay Minerals Society (2004, 2006) and the AAPG (John Teagle Memorial Grant, 2004) to DPJ. The authors are grateful to three anonymous reviewers and the Associate Editor whose comments greatly improved the quality of the manuscript.

REFERENCES

Ahn, J.H. and Peacor, D.R. (1989) Illite/smectite from Gulf Coast shales: A reappraisal of transmission electron microscope images. *Clays and Clay Minerals*, **27**, 542−546.

Anastacio, A.S., Harris, B., Yoo, H.-I., Fabris, J.D., and Stucki,

J.W. (2008) Limitations of the ferrozine method for quantitative assay of mineral systems for ferrous and total iron. *Geochimica et Cosmochimica Acta*, **21**, 5001–5008.

Balkwill, D.L., Kieft, T.L., Tsukuda, T., Kostandarithes, H.M., Onstott, T.C., Macnaughton, S., Bownas, J. and Fredrickson, J.K. (2004) Identification of iron-reducing *Thermus* strains as *Thermus scotoductus*. *Extremophiles*, **8**, 37–44.

Bauer, A. and Velde, B. (1999) Smectite transformation in high molar KOH solutions. *Clay Minerals*, **34**, 259–273.

Bethke, C.M., Harrison, W.J., Upson, C., and Altaner, S.P. (1988) Supercomputer analysis of sedimentary basins. *Science*, **237**, 261–267.

Bjørkum, P.A. and Nadeau, P.H. (1998) Temperature controlled porosity/permeability reduction, fluid migration, and petroleum exploration in sedimentary basins. *APEAJ*, 453–464.

Blum, A.E. and Eberl, D.D. (2004) Measurement of clay surface area by polyvinyl pyrrolidone (PVP) sorption and its use for quantifying illite and smectite. *Clays and Clay Minerals* **52**, 589–602.

Boles, J.R. and Franks, S.G. (1979) Clay diagenesis in Wilcox sandstones of southwest Texas: Implications of smectite diagenesis on sandstone cementation. *Journal of Sedimentary Petrology*, **49**, 55–70.

Brown, K.M., Saffer, D.M. and Bekins, B.A. (2001) Smectite diagenesis, pore-water freshening, and fluid flow at the toe of the Nankai wedge. *Earth and Planetary Science Letters*, **194**, 97–109.

Bruce, C.H. (1984) Smectite dehydration – its relation to structural development and hydrocarbon accumulation in Northern Gulf of Mexico Basin. *AAPG Bulletin*, **68**, 673–683.

Burst, J.F. (1969) Diagenesis of Gulf Coast clayey sediments and its possible relation to petroleum migration. *AAPG Bulletin*, **53**, 73–93.

Claret, F., Bauer, A., Schäfe, T., Griffault, L., and Lanson, B. (2002) Experimental investigation of the interaction of clays with high pH solutions: A case study from the Callovo-Oxfordian formation, Meuse-Haute Marne underground Laboratory (France). *Clays and Clay Minerals*, **50**, 633–646.

Cuadros, J. (2006) Modeling of smectite illitization in burial diagenesis environments. *Geochimica et Cosmochimica Acta*, **70**, 4181–4195.

Cuadros, J. and Linares, J. (1998) Experimental kinetic study of the smectite-to-illite transformation. *Geochimica et Cosmochimica Acta*, **60**, 439–463.

Dong, H. (2005) Interstratified illite-smectite: a review of contributions of TEM data to crystal chemical relation and reaction mechanisms. *Clay Science*, **12**, 6–12.

Dong, H., Kostka, J.E. and Kim, J.W. (2003) Microscopic evidence for microbial dissolution of smectite. *Clays and Clay Minerals*, **51**, 502–512.

Dong, H., Peacor, D.R. and Freed, R.L. (1997) Phase relations among smectite, R1 I/S and illite. *American Mineralogist*, **82**, 379–391.

Dong, H., Jaisi, D.P., Kim, J., and Zhang, G. (2009) Microbe-clay mineral interactions. *American Mineralogist*, **94**, 1505–1519.

Drief, A., Martinez-Ruiz, A., Nieto, F., and Velilla Sanchez, N. (2002) Transmission electron microscopy evidence for experimental illitiztion of smectite in K-enriched seawater solution at 50ºC and basic pH. *Clays and Clay Minerals*, **50**, 746–456.

Drits, V.A., Środoń, J., and Eberl, D.D. (1997) XRD measurement of mean crystallite thickness of illite and illite/smectite: Reappraisal of the Kübler index and the Scherrer equation. *Clays and Clay Minerals*, **45**, 461–475.

Drits, V.A., Eberl, D.D., and Środoń, J. (1998) XRD measurement of mean thickness, thickness distribution and strain for illite and illite-smectite crystallites by the Bertaut-Warren-Averbach technique. *Clays and Clay Minerals*, **46**, 38–50.

Eberl, D.D., Środoń, J., and Northrop, H.R. (1986) Potassium fixation in smectite by wetting and drying. *Geochemical Processes at Mineral Surfaces.* American Chemical Society Symposium, **323**, 296–326.

Eberl, D.D., Drits, V.A., Środoń, J., and Nuesch, R. (1996) MUDMASTER: A program for calculating crystallite size distributions and strain from the shapes of X-ray diffraction peaks. *U.S. Geological Survey, Open-File Report 96-171.*

Eberl, D.D., Nuesch, R., Śucha, V., and Tsipursky, S. (1998) Measurement of fundamental illite particle thicknesses by X-ray diffraction using PVP-10 intercalation. *Clays and Clay Minerals*, **46**, 89–97.

Fredrickson, J.K., Zachara, J.M., Kennedy, D.W., Dong, H.L., Onstott, T.C., Hinman, N.W., and Li, S.M. (1998) Biogenic iron mineralization accompanying the dissimilatory reduction of hydrous ferric oxide by a groundwater bacterium. *Geochimica et Cosmochimica Acta*, **62**, 3239–3257.

Freed, R.L. and Peacor, D.R. (1989) Geopressured shale and sealing effect of smectite to illite transition. *AAPG Bulletin*, **73**, 1223–1232.

Furukawa, Y. and O'Reilly, S.E. (2007) Rapid precipitation of amorphous silica in experimental systems with nontronite (NAu-1) and *Shewanella oneidensis* MR-1. *Geochimica et Cosmochimica Acta*, **71**, 363–377.

Fysh S. and Clark P.E. (1982) Aluminous Goethite: A Mössbauer Study. *Physics and Chemistry of Minerals*, **8**, 180–187.

Gates, W.P., Wilkinson, H.T., and Stucki, J.W. (1993) Swelling properties of microbially reduced ferruginous smectite. *Clays and Clay Minerals*, **41**, 360–364.

Gates, W.P., Jaunet, A.M., Tessier, D., Cole, M.A., Wilkinson, H.T., and Stucki, J.W. (1998) Swelling and texture of iron-bearing smectites reduced by bacteria. *Clays and Clay Minerals*, **46**, 487–497.

Glasmann, J.R., Clark, R.A., Larter, S., Briedis, N.A., and Lundegard, P.D. (1989) Diagenesis and hydrocarbon accumulation, Brent Sandstone (Jurassic), Bergen High Area, North Sea. *AAPG Bulletin*, **73**, 1341–1360.

Howard, J.J. (1981) Lithium and potassium saturation of illite/smectites clay from laminated shales and sandstones. *Clays and Clay Minerals*, **2**, 136–142.

Hower, J., Eslinger, E.V., Hower, M.H., and Perry, E.A. (1976) Mechanism of burial metamorphism of argillaceous sediments. 1. Mineralogical and chemical evidence. *Geological Society of America Bulletin*, **87**, 725–737.

Huang, W.L., Longo, J.M., and Pevear, D.R. (1993) An experimentally derived kinetic model for smectite-to-illite conversion and its use as a geothermometer. *Clays and Clay Minerals*, **41**, 162–177.

Jaisi, D.P., Kukkadapu, R.K., Eberl, D.D., and Dong, H.L. (2005) Control of Fe(III) site occupancy on the rate and extent of microbial reduction of Fe(III) in nontronite. *Geochimica et Cosmochimica Acta*, **69**, 5429–5440.

Jaisi, D.P., Dong, H., and Liu, C. (2007a) Influence of biogenic Fe(II) on the extent of microbial reduction of Fe(III) in clay minerals nontronite, illite, and chlorite. *Geochimica et Cosmochimica Acta*, **71**, 1145–1158.

Jaisi, D. P., Dong, H., and Liu, C. (2007b) Kinetic analysis of microbial reduction of Fe(III) in nontronite. *Environmental Science and Technology*, **41**, 2437–2444.

Jaisi, D.P., Dong, H., and Morton, J.P. (2008) Partitioning of Fe(II) in reduced nontronite (NAu-2) to reactive sites: Reactivity in terms of Tc(VII) reduction. *Clays and Clays Minerals*, **56**, 175–189.

Kaufhold, S. and Dohrmann, R. (2010) Stability of bentonites

in salt solutions: II. Potassium chloride solution – Initial step of illitization? *Applied Clay Science*, **49**, 98–107.

Keeling, J.L., Raven, M.D., and Gates, W.P. (2000) Geology and characterization of two hydrothermal nontronites from weathered metamorphic rocks at the Uley Graphite Mine, South Australia. *Clays and Clay Minerals*, **48**, 537–548.

Kieft, T.L., Fredrickson, J.K., Onstott, T.C., Gorby, Y.A., Kostandarithes, H.M., Bailey, T.J., Kennedy, D.W., Li, S.W., Plymale, A.E., Spadoni, C.M., and Gray, M.S. (1999) Dissimilatory reduction of Fe(III) and other electron acceptors by a *Thermus* isolate. *Applied and Environmental Microbiology*, **65**, 1214–1221.

Kim, J.W., Peacor, D.R., Tessier, D., and Elsass, F. (1995) A technique for maintaining texture and permanent expansion of smectite interlayers for TEM observations. *Clays and Clay Minerals*, **43**, 51–57.

Kim, J.W., Bryant, W.R., Watkins, J., and Tieh, T.T. (1999) Electronmicroscopic observations of shale diagenesis, Offshore Louisiana, USA, Gulf of Mexico: *Geo-Marine Letters*, **18**, 234–240.

Kim, J.W., Newell, S., Furukawa, Y., Lavoie, D., and Daulton, T. (2003) Characterization of microbially Fe(III)-reduced nontronite: environmental cell transmission electron microscopy. *Clays and Clay Minerals*, **51**, 382–389.

Kim, J.W., Dong, H., Seabaugh, J., Newell, S.W., and Eberl, D.D. (2004) Role of microbes in the smectite-to-illite reaction. *Science*, **303**, 830–832.

Kim, J.W., Furukawa, Y., Dong, H., and Newell, S.W. (2005) The effect of microbial Fe(III) reduction in the clay flocculation. *Clays and Clay Minerals*, **53**, 572–579.

Kostka, J.E., Stucki, J.W., Nealson, K.H., and Wu, J. (1996) Reduction of structural Fe(III) in smectite by a pure culture of *Shewanella putrefaciens* strain MR-1. *Clays and Clay Minerals*, **44**, 522–529.

Kostka, J.E., Haefele, E., Viehweger, R., and Stucki, J.W. (1999a) Respiration and dissolution of iron(III)-containing clay minerals by bacteria. *Environmental Science and Technology*, **33**, 3127–3133.

Kostka, J.E., Wu, J., Nealson, K.H., and Stucki, J.W. (1999b) The impact of structural Fe(III) reduction by bacteria on the surface chemistry of smectite clay minerals. *Geochimica et Cosmochimica Acta*, **63**, 3705–3713.

Lahann, R.W. (1980) Smectite diagenesis and sandstone cement: The effect of reaction temperature. *Journal of Sedimentary Research*, **50**, 755–760.

Larese-Casanova, P., Cwiertny, D.M., and Scherer, M.M. (2010) Nanogoethtie formation from oxidation of Fe(II) sorbed on alumnium oxide: Implications for contaminant reduction. *Environmental Science and Technology*, **44**, 3765–3771.

Li, H., Teppen, B.J., Laird, D.A., Johnston, C.T., and Boyd, S.A. (2004) Geochemical modulation of pesticide sorption on smectite clay. *Environmental Science and Technology*, **38**, 5393–5399.

Li, Y.L., Vali, H., Sears, S.K., Yang, J., Deng, B., and Zhang, C. (2004) Iron reduction and alteration of nontronite NAu-2 by a sulfate reducing bacterium. *Geochimica et Cosmochimica Acta*, **68**, 3251–3260.

Lovley, D., Holmes, K.P. and Nevin, D.E. (2004) Dissimilatory Fe(III) and Mn(IV) reduction. *Advances in Microbial Physics*, **49**, 219–287.

Moller, C. and van Heerden, E. (2006) Isolation of a soluble and membrane-associated Fe(III) reductase from the thermophile, *Thermus scotoductus* (SA-01). *FEMS Microbiology Letters*, **265**, 237–243.

Moore, D.M. and Reynolds, R.C., Jr. (1997) *X-ray Diffraction and the Identification and Analysis of Clay Minerals*. Oxford University Press, New York.

Murad, E. and Cashion, J. (2004) *Mössbauer Spectroscopy of Environmental Materials and their Industrial Utilization*. Kluwer Academic Publishers, Boston, Massachusetts, USA, 440 pp.

Peacor, D.R. (1992) Analytical electron microscopy: X-ray Analysis. Pp. 335–380 in: *Minerals and Reactions at the Atomic Scale: Transmission Electron Microscopy* (P.R. Bruseck, editor). Reviews in Mineralogy, **27** (P. Buseck, editor). Mineralogical Society of America, Washington, D.C.

Pevear, D.R. (1999) Illite and hydrocarbon exploration. *Proceedings of the National Academy of Sciences of the United States of America*, **96**, 3440–3446.

Pollastro, R.M. (1985) Mineralogical and morphological evidence for the formation of illite at the expense of illite/smectite. *Clays and Clay Minerals*, **33**, 265–274.

Pollastro, R.M. (1993) Considerations and applications of the illite/smectite geothermometer in hydrocarbon-bearing rocks of Miocene to Mississippian age. *Clays and Clay Minerals*, **41**, 119–133.

Pytte, A.M. and Reynolds, R.C., Jr. (1989) The thermal transformation of smectite to illite. Pp. 133–140 in: *Thermal History of Sedimentary Basins: Methods and Case Histories* (N.D. Naeser and T.H. McCulloh, editors). Springer-Verlag, New York.

Reynolds, R.C. (1985) *NEWMOD©*, A Computer Program for the Calculation of One-Dimensional Diffraction Patterns of Mixed-Layered Clays. 8 Brook Road, Hanover, New Hampshire, USA 03755.

Seabaugh, J.L., Dong, H., Kukkadapu, R.K., Eberl, D., Morton, J.P., and Kim, J.W. (2006) Microbial reduction of Fe(III) in the Fithian and Muloorina illites: contrasting extents and rates of bioreduction. *Clays and Clay Minerals*, **54**, 67–79.

Środoń, J. (1980) Precise identification of illite/smectite interstratification by X-ray powder diffraction. *Clays and Clay Minerals*, **28**, 401–411.

Stixrude, L. and Peacor, D.R. (2002) First-principles study of illite-smectite and implications for clay mineral systems. *Nature*, **420**, 165–168.

Stookey, L.L. (1970) Ferrozine – A new spectrophotometric reagent for Iron. *Analytical Chemistry*, **42**, 779–187.

Stucki, J.W. and Kostka, J.E. (2006) Microbial reduction of iron in smectite. *Geoscience*, **338**, 468–475.

Veblen, D.R., Guthrie, G.D., Livi, K.T., and Reynolds, R.C., Jr. (1990) High-resolution transmission electron microscopy and electron diffraction of mixed-layer illite/smectite: experimental results. *Clays and Clay Minerals*, **38**, 1–13.

Vorshies, J.S. and Gaines, R.R. (2009) Microbial dissolution of clay minerals as a source of iron and silica in marine sediments. *Nature Geoscience*, **2**, 221–225.

Weaver, C.E. (1960) Possible uses of clay minerals in the search for oil. *AAPG Bulletin*, **44**, 1505–1518.

Weaver, C.E. and Beck, K.C. (1971) Clay water diagenesis during burial, how mud becomes gneiss. *Geological Society of America Special Paper*, **134**, 96.

Whitney, G. (1990) Role of water in the smectite to illite reaction. *Clays and Clay Minerals*, **38**, 343–350.

Wintsch, R.P. and Kvale, C.M. (1994) Differential mobility of elements in burial diagenesis of siliciclastic rocks. *Journal of Sedimentary Research*, **64**, 349–361.

Zachara, J.M., Fredrickson, J.K., Li, S.W., Kennedy, D.W., Smith, S.C., and Gassman, P.L. (1998) Bacterial reduction of crystalline Fe^{3+} oxides in single phase suspensions and subsurface materials. *American Mineralogist*, **83**, 1426–1443.

Zhang, G., Kim, J.W., Dong, H., and Sommer, A.J. (2007a) Microbial effects in promoting the smectite to illite reaction: role of organic matter intercalated in the interlayer. *American Mineralogist*, **92**, 1401–1410.

Zhang, G., Dong, H., Kim, J.W. and Eberl, D.D. (2007b)

Microbial reduction of structural Fe(III) in nontronite by a thermophilic bacterium and its role in promoting the smectite to illite reaction. *American Mineralogist*, **92**, 1411–1419.

Zhang, G., Senko, J.M., Kelly, S.D., Tan, H., Kemner, K.M., and Bufgos, W.D. (2009) Microbial reduction of iron(III)-rich nontronite and uranium(VI). *Geochimica et Cosmochimica Acta*, **73**, 3523–3538.

Zhao, J., Huggins, F.E., Feng, Z., and Huffman, G.P. (1996) Surface-induced superparamagnetic relaxation in nanoscale ferrihydrite particles. *Physical Review B*, **54**, 3403–3407.

(*Received 23 April 2010; revised 7 February 2011; Ms. 430; A.E. R. Dohrmann*)